ACS APPLIED MATERIALS & INTERFACES
Research Article
www.acsami.org

Effect of Indium Segregation on the Surface versus Bulk Chemistry for Indium-Doped TiO_2

Armand J. Atanacio,[†,‡] Tadeusz Bak,[‡] and Janusz Nowotny*[,‡]

[†]Australian Nuclear Science and Technology Organisation, Locked Bag 2001, Kirawee DC, New South Wales 2232, Australia
[‡]Solar Energy Technologies, University of Western Sydney, Penrith, New South Wales 2751, Australia

ABSTRACT: This work reports the effect of indium segregation on the surface versus bulk composition of indium (In)-doped TiO_2. The studies are performed using proton-induced X-ray emission (PIXE), secondary-ion mass spectrometry (SIMS), X-ray photoelectron spectroscopy (XPS), and Rutherford backscattering spectroscopy (RBS). The results of XPS analysis indicate that annealing of In-doped TiO_2 containing 0.3 atom % In at 1273 K in the gas phase of controlled oxygen activity [$p(O_2)$ = 75 kPa and 10 Pa] results in a surface enrichment of 2.95 and 2.61 atom % In, respectively. The obtained segregation data are considered in terms of the transport of indium ions from its titanium sites in the bulk phase to the surface where these ions are incorporated into interstitial sites. The effect of oxygen activity on the segregation-induced surface enrichment is considered in terms of the formation of a low-dimensional surface structure and a sublayer, which are charged negatively. The latter is formed as a result of strong interactions between titanium vacancies and interstitial indium ions, leading to the formation of defect complexes. The data obtained in this work may be used for engineering of TiO_2-based semiconductors with enhanced performance in solar energy conversion.

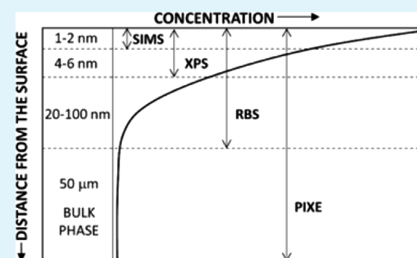

KEYWORDS: *titanium dioxide, rutile, segregation, indium, surface structure, defect disorder*

1. INTRODUCTION

TiO_2 is a promising candidate for the photocatalytic removal of toxic organic contaminants from water[1,2] and the photoelectrochemical generation of hydrogen fuel from water.[3] The first successful experiment of Fujishima and Honda[3] on photoelectrochemical water splitting resulted in intensive research, which aims at the modification of TiO_2 in order to enhance its performance. The ultimate goal of the research is to form a TiO_2-based system that is able to perform at the level of efficiency that is required for commercialization.

The most common way to modify the performance-related properties of oxides, including TiO_2, such as the electronic structure, flat band potential, and surface properties, is the incorporation of aliovalent ions into the TiO_2 lattice (doping).[4−8] The process of doping, which results in the formation of donor and/or acceptor centers, leads to a change in the concentration of electronic charge carriers and related semiconducting properties in a controlled manner. So far, the effect of doping on the properties of oxides has been mainly considered in terms of bulk properties. Awareness is growing, however, that the mechanism of incorporation of foreign ions and the resulting properties of the bulk phase and surface can be entirely different.[9−12] Clarification of this effect is crucial for correctly understanding the effect of doping on the performance of photoelectrodes and photocatalysts, which is determined by the surface versus bulk properties. So far, however, little is known in this matter.

There has been an accumulation of reports indicating that solutes in the bulk phase segregate to the surface; however, the reported enrichment data are conflicting.[13] Moreover, awareness is growing that segregation of solutes in metal oxides is profoundly influenced by intrinsic defect disorder and the related oxygen activity.[9−11] Therefore, there is an increasingly urgent need to understand the effect of segregation on both the bulk and surface properties of oxides and, specifically, the effect of oxygen activity on segregation-induced enrichment.

The present work is part of a larger research program to investigate the effect of segregation on the surface properties of photosensitive oxide semiconductors, including chemical composition and the associated performance-related properties of TiO_2 solid solutions with donor- and acceptor-type ions.

Our previous work for indium (In)-doped TiO_2 has revealed that the effect of indium segregation on the surface composition is a compromise between indium evaporation and segregation.[14] That work resulted in the following conclusions:

Equilibrium Segregation. The determination of equilibrium segregation requires knowledge of the time needed to establish equilibrium. It was shown that equilibrium segregation of indium in the TiO_2 lattice in an oxidizing atmosphere at 1273 K can be reached within 20 h.

Evaporation. Annealing of In-doped TiO_2 in a strongly reducing environment does not lead to equilibrium segregation because of indium evaporation. In this case, the resulting surface concentration of indium is a compromise between the rate of segregation and the rate of evaporation. Knowledge of these effects may be used to set up appropriate processing

Received: August 24, 2012
Accepted: November 12, 2012
Published: November 12, 2012

© 2012 American Chemical Society

conditions for the formation of well-defined In-doped TiO_2 in terms of the surface versus bulk composition.

The purpose of the present work is, using the experimental framework established previously,[14] to determine the effect of indium segregation on the surface versus bulk composition of In-doped TiO_2 in an oxidizing environment. In this environment, the segregation-induced surface composition is not affected by evaporation. In order to establish the effect of segregation on the local indium concentration within the surface layer, it seems appropriate to use the following range of analytical tools, which exhibit different sensitivity to the surface versus bulk composition:

(1) *Secondary-ion mass spectrometry (SIMS).* This destructive method is extremely sensitive to the chemical composition. This technique is able to analyze the composition-related intensity data in lattice layers of approximately 1 nm in thickness, which can be removed layer-by-layer up to 10 μm in depth. However, a quantitative assessment of the SIMS intensity data in terms of the lattice composition versus depth requires akward calibration. Furthermore, SIMS can be strongly influenced by matrix-related effects, which add further complexity. Consequently, SIMS is typically utilized for qualitative depth profiling.

(2) *X-ray photoelectron spectroscopy (XPS).* This method, which is nondestructive, provides information on the absolute values of the surface layer composition within 4−6 nm, depending on the angle of incidence.

(3) *Rutherford backscattering spectroscopy (RBS).* The analysis depth of this method, which is also nondestructive, is on the order of tens of nanometers and, therefore, is larger than that of SIMS and XPS. In the case of RBS, the smallest analysis depth can be as low as 20−30 nm and the probing depth as large as 2 μm. Therefore, RBS is a less surface-sensitive technique than SIMS and XPS.

(4) *Proton-induced X-ray emission (PIXE).* The analysis depth of PIXE is on the order of tens of micrometers and provides no information in relation to the concentration as a function of the depth. Therefore, unlike SIMS, XPS, and RBS, PIXE is mainly sensitive to the composition of the bulk phase.

Because these techniques have different sensitivity to the surface composition, the related data may be used for derivation of a reliable picture on the effect of segregation on the surface versus bulk composition. The experimental part of this work is preceded by a brief analysis of literature reports and definitions of basic terms.

2. LITERATURE REPORTS

There have been several attempts to understand the effect of indium on a wide range of the TiO_2 properties.

Nakamura et al.[15] reported the effect of indium introduced into the TiO_2 lattice by implantation. They observed that implantation and subsequent annealing result in the formation of titanium interstitials. This effect suggests that indium is incorporated predominantly into titanium sites, forming acceptors, which are compensated by titanium interstitials and oxygen vacancies. They claim that when the concentration of indium in titanium sites surpasses a certain critical limit (72−88%), the remaining fraction of indium ions is incorporated into interstitial sites.

Babu et al.[16] reported that the formation of a TiO_2 solid solution with In_2O_3 (by powder sintering during 24 h at 1273 K) results in a change of a wide range of properties including (i) a reduction of the band gap, (ii) a shift in the flat band potential, (iii) an increase in the surface area, and (iv) enhanced photoassisted hydrogen evolution.

Sasikala et al.[17] observed that codoping of TiO_2 with indium and nitrogen results in band-gap narrowing due to mixing of the energy levels and leading, as a consequence, to enhanced photocatalytic activity. On the other hand, Wang et al.[18] reported that indium doping does not result in a change of the band gap of TiO_2. Instead, they observed the formation of a surface chemical structure O−In−Cl_x, with the energy level 0.3 eV below the conduction band. They claim that this structure allows more efficient utilization of visible light and enhancement of charge separation.

Rodriguez-Gonzales et al.[19] studied two mixed-oxide systems; (i) one formed by mixing TiO_2 and In_2O_3 by sol−gel (calcined at 773 K) and (ii) the other In_2O_3/TiO_2 system formed by impregnating TiO_2 gel (calcined at 773 K) with a solution of indium acetylacetonate acetone. They observed that the mixed and impregnated systems exhibit band gaps of 3.5 and 3.1 eV, respectively. They also observed that the mixed system, involving highly dispersed In_2O_3, exhibits higher photocatalytic activity, which they attributed to better charge separation. Similar effects were reported by Rangel-Porras et al.,[20] who observed that the presence of indium during the formation of TiO_2 by sol−gel results in a highly mesoporous microstructure.

Using the periodic plane-wave density functional theory, Iwaszuk and Nolan[21] determined that the incorporation of indium into the lattice of TiO_2 results in the formation of acceptor centers that are compensated by oxygen vacancies. The substitutional mechanism of indium incorporation into the bulk phase has been confirmed by recent studies on the effect of indium on the semiconducting properties in terms of both electrical conductivity and thermoelectric power data.[22]

In summary, the literature reports indicate that indium in the bulk phase of TiO_2 is incorporated predominantly into titanium sites, leading to the formation of acceptors. However, the experiment of Nakamura et al.[15] suggests that a small fraction of indium is incorporated into interstitial sites.

3. DEFINITION OF TERMS

3.1. Defect Disorder.

This section considers TiO_2 defect disorder using the Kröger−Vink[23] notation, which is defined in Table 1. The related defect equilibria are defined in Table 2.[1]

It has been documented that the photoreactivity of oxide semiconductors, such as TiO_2, is closely related to defect disorder. Therefore, their photoreactivity and related performance can be modified by shifting the defect equilibria.

Table 1. Kröger−Vink[23] and Traditional Notation of Defects for TiO_2

traditional notation	description	Kröger−Vink notation
Ti_{Ti}^{4+}	Ti_{Ti}^{4+} ion in the titanium lattice site	Ti_{Ti}^{x}
Ti_{Ti}^{3+}	Ti_{Ti}^{3+} ion in the titanium lattice site (quasi-free electron)	e'
V_{Ti}	titanium vacancy	V_{Ti}''''
Ti_i^{3+}	Ti_i^{3+} in the interstitial site	$Ti_i^{\bullet\bullet\bullet}$
Ti_i^{4+}	Ti_i^{4+} in the interstitial site	$Ti_i^{\bullet\bullet\bullet\bullet}$
O_O^{2-}	O_O^{2-} ion in the oxygen lattice site	O_O^{x}
V_O	oxygen vacancy	$V_O^{\bullet\bullet}$
O_O^{-}	O_O^{-} ion in the oxygen lattice site (quasi-free electron hole)	$h^{\bullet}$

dx.doi.org/10.1021/am301729z | *ACS Appl. Mater. Interfaces* 2012, 4, 6626−6634

Table 2. Basic Defect Equilibria in TiO_2[1] Described Using the Kröger–Vink[23] Notation

	defect reaction	equilibrium constant	$\Delta H°$ (kJ/mol)	$\Delta S°$ [J/(mol·K)]
1	$O_O^x \Leftrightarrow V_O^{\bullet\bullet} + 2e' + \frac{1}{2}O_2$	$K_1 = [V_O^{\bullet\bullet}]n^2 p(O_2)^{1/2}$	493.1	106.5
2	$Ti_{Ti}^x + 2O_O^x \Leftrightarrow Ti_i^{\bullet\bullet\bullet} + 3e' + O_2$	$K_2 = [Ti_i^{\bullet\bullet\bullet}]n^3 p(O_2)$	879.2	190.8
3	$Ti_{Ti}^x + 2O_O^x \Leftrightarrow Ti_i^{\bullet\bullet\bullet\bullet} + 4e' + O_2$	$K_3 = [Ti_i^{\bullet\bullet\bullet\bullet}]n^4 p(O_2)$	1025.8	238.3
4	$O_2 \Leftrightarrow V_{Ti}'''' + 4h^{\bullet} + 2O_O^x$	$K_4 = [V_{Ti}'''']p^4 p(O_2)^{-1}$	354.5	−202.1
5	$\text{nil} \Leftrightarrow e' + h^{\bullet}$	$K_i = np$	222.1	44.6

$\ln K = [(S°)/R] - [(H°)/RT]$

The effect of indium on the semiconducting properties of TiO_2 depends on the mechanism of its incorporation. The incorporation of indium into TiO_2 may be represented by the reaction

$$In_2O_3 \rightarrow 2In_{Ti}' + 3O_O^x + V_O^{\bullet\bullet} \quad (1)$$

This defect disorder is governed by ionic charge compensation of indium:

$$[In_{Ti}'] = 2[V_O^{\bullet\bullet}] \quad (2)$$

The combination of the equilibrium constants K_1 and K_i and the relation (2) result in the following relation between the concentration of electronic charge carriers and oxygen activity:

$$p = K_i\left(\frac{[In_{Ti}']}{2K_1}\right)^{1/2} p(O_2)^{1/4} \quad (3)$$

The incorporation of indium into the TiO_2 lattice at high oxygen activities leads to the formation of electron holes:

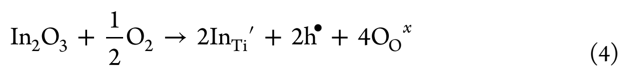

$$In_2O_3 + \frac{1}{2}O_2 \rightarrow 2In_{Ti}' + 2h^{\bullet} + 4O_O^x \quad (4)$$

Consequently, this regime is governed by the following charge compensation:

$$[In_{Ti}'] = p \quad (5)$$

The effect of acceptor-type ions on the bulk defect disorder of TiO_2 can be considered in terms of a Brouwer-type defect diagram.[24]

The relations (1)–(5) represent the theoretical background on the effect of indium on the bulk properties of TiO_2 in terms of defect chemistry. It is important to note that the effect of indium doping on the surface properties of TiO_2 may be entirely different because of the effect of segregation. The aim of the present work is to determine the effect of indium segregation on the bulk versus surface composition of TiO_2. This will be achieved by determination of the indium concentration in the bulk phase and at the surface using a range of analytical techniques: SIMS, XPS, RBS, and PIXE. The related data will be considered in terms of defect chemistry independently for the bulk phase and surface layer.

3.2. Diffusion of Indium in TiO_2 (Rutile). The effect of doping with a foreign ion is well-defined only when the transport kinetics of this ion, resulting in incorporation, is well-defined. Therefore, this work was preceded by determination of the diffusion kinetics of indium in the TiO_2 lattice.[26] The obtained diffusion data were then used to assess the appropriate annealing conditions that allow homogeneous distribution of indium in the specimen.

3.3. Segregation. Surface segregation is the diffusion of certain lattice elements from the bulk phase to the surface, leading to surface enrichment in these elements. The driving force of segregation is the excess of surface energy.

The studies of segregation in oxides, such as NiO and CoO, indicate that both intrinsic defects, such as oxygen and cation vacancies, and extrinsic defects segregate to the surface.[11] Therefore, interaction between both types of defects should be taken into account when considering the kinetics of segregation and its effect on the surface properties. It has been documented that the segregation-induced enrichment of the surface layer of oxide solid solutions, such as chromium (Cr)-doped CoO, may substantially surpass the bulk solubility limit.[25] In certain cases, the segregation-induced enrichment of the surface layer results in the formation of low-dimensional surface structures.[10,26] This is the case when the local concentrations surpass certain critical limits. The critical concentrations not only depend on the surface structure, which is different from that of the bulk phase as a result of the broken crystalline periodicity, but also depend on the intrinsic defect disorder. The latter, in the case of metal oxides, is profoundly influenced by the oxygen activity.

The purpose of the present work is to assess the segregation-induced surface concentration of indium in In-doped TiO_2, understand the predominant driving force of segregation, and determine the effect of oxygen activity on segregation.

4. EXPERIMENTAL SECTION

4.1. Specimens. In-doped TiO_2 was prepared by the sol–gel technique using titanium isopropoxide, indium chloride, acetic acid, ethanol, and water. The amounts of acetic acid, water, and titanium isopropoxide were adjusted to achieve the final molar ratio of 1.5:1 acetic acid to titanium and 4:1 water to titanium.[27] The total amount of ethanol was adjusted to achieve 0.8 mol/L in the final solution.[27] The total amount of $InCl_3$ powder was added to achieve several concentrations of indium in the range 0.02–2.5 atom %. The $InCl_3$ powder was mixed with a small volume of ethanol in a beaker (B1) and stirred until fully dissolved. $Ti[OCH(CH_3)_2]_4$ was combined under stirring with acetic acid (used as a chelating agent) in a second beaker (B2). In a third beaker (B3), the remaining amount of ethanol was mixed with deionized water. The B1 solution was slowly added to the (B2) solution under stirring, and after 1 h, the (B3) solution was added (dropwise) to the B2 solution. The resulting gel was placed on a hot plate (80 °C) and left to dry for 2 or 3 days. The solid product (solid solution) was then ground into a fine powder, which was placed in a platinum-lined alumina boat and calcined in air in a tube furnace at 1173 K. The calcined powder was then pressed into cylindrical pellets, initially using a uniaxial press and subsequently using a cold isostatic press at 400 MPa. The pressed pellets were sintered in air at 1773 K for 5 h. Finally, a surface layer (~30–50 μm) was removed by polishing. The resulting *as-polished* specimen is considered as a reference specimen.

dx.doi.org/10.1021/am301729z | ACS Appl. Mater. Interfaces 2012, 4, 6626–6634

The *as-polished* specimens were then annealed at 1273 K for 24 h in a gas phase of well-defined oxygen activities to induce segregation: pure oxygen, $p(O_2)$ = 75 kPa; pure argon, $p(O_2)$ = 10 Pa.

The required oxygen activity was imposed by flowing appropriate gases through the reactor (tube furnace) with a flow rate of 100 mL/min. The oxygen activity in the reactor was monitored electrochemically during the entire experiment using the zirconia oxygen probe.

4.2. Bulk Analysis. *X-ray Diffraction (XRD).* XRD analysis (Siemens D500) was performed using a Co $K\alpha_{1,2}$ radiation source and a graphite monochromator. Data were collected over the angular range of 5−80° with a 2θ step size of 0.05 and a 5 s dwell time. The PANalytical software package was used for identification of the crystalline phases. The obtained XRD patterns are shown in Figure 1.

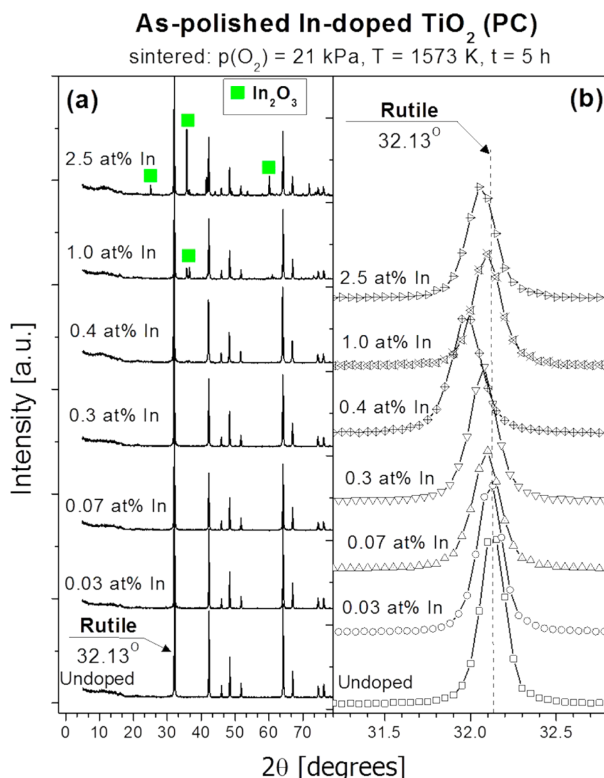

Figure 1. XRD patterns for In-doped TiO_2. This pattern, showing the peaks related to a phase other than rutile, indicates that the solubility range of indium in rutile is approximately 1 atom %.

As seen, the X-ray spectra are reflective of the rutile structure for In-doped TiO_2 up to 0.4 atom % In. As is also seen, traces of the In_2O_3 phase are detected at 1 and 2.5 atom %. These data indicate that the solubility of indium in rutile is between 0.4 and 1 atom % In. It is important to note that this solubility limit concerns the bulk phase.

PIXE. PIXE analysis was performed at the Australian Nuclear Science and Technology Organisation using a 2MV STAR tandem accelerator. The technical specification for PIXE analysis is as follows:

Sample Charge. The charge collected for each sample was 30 μC.

Detector. The X-rays were recorded at a 45° angle using a Si(Li) detector fitted with a 25 μm beryllium window and a multichannel energy analyzer.

Filter. An additional pinhole acrylic filter, 1700 μm thick, with a 2% hole area and a 4-μm-thick mylar film, which aimed at decreasing the intensity of low-energy X-rays excited with high cross sections, was placed over the X-ray detector to minimize pileup and deadtime during analysis.

Data Processing. The PIXE spectra were processed using the *GUPIXWIN* (version 2.1.4) software package for determination of the elemental concentrations. Quantitative analysis of the indium peaks is related to a depth of 42 μm (based on the proton penetration range in TiO_2 determined using the *SRIM* software program).

4.3. Surface Analysis. *SIMS.* The SIMS depth profiles were determined using SIMS (Cameca IMS 5f). A Cs^+ primary ion beam of 5 nA current and 5 keV net impact energy was used to raster the area of 250 × 250 μm and sputter secondary ions. Sample charging was reduced by deposition of a thin layer of gold (∼5 nm) on the sample surface. The depth of the crater after analysis (measured using a profilometer) was used for determination of the average sputter rate (time vs depth). The sputter rate was 0.012 nm/s. SIMS electronic gating settings were used to restrict secondary-ion analysis to a 55 μm circular area within the rastered region to avoid the influence of crater edge effects on the results.

The SIMS technique provides depth profiles in terms of ion intensity (counts). The absolute concentration values can be determined from the intensity of the species of interest divided by those for species whose intensity remains relatively constant throughout the specimen such as the host (matrix) species (TiO). The atom proportion of indium to titanium can be determined from the peak-height proportion of $^{115}In/(^{48}Ti + ^{16}O)$ in the mass spectrum, according to the following formula:

$$\frac{C_{In}}{C_{TiO}} = \frac{I_{In}K_{TiO}{}^{+}h_{TiO}}{I_{TiO}K_{In}{}^{+}h_{In}} \tag{6}$$

where I is the ion intensity, K^+ is the secondary-ion yield (defined as the number of secondary ions produced per incident primary ion of mass m and charge $z\pm$), and h is the isotopic abundance.[28] The form (6) may be reduced to the following form:

$$C_{In} = \frac{I_{In}}{I_{TiO}}F_{In} \tag{7}$$

where F_{In} is a calibration factor. The calibration factor is not solely related to the species of interest but is influenced by a complex contribution of the host matrix composition and structure (including density, crystal orientation, or grain boundaries) as well as the SIMS sputtering conditions used (including primary ion, beam current, and impact energy). Consequently, determination of the calibration factor typically requires generation of a calibration curve using reference samples containing known concentrations of the species of interest in the same matrix as the unknown samples and analyzed under the same SIMS conditions. However, even without the quantitative calibration factor, the SIMS depth profiles can still be used for semiquantitative analysis.

XPS. XPS analysis was performed using a Thermo Scientific ESCALAB 250xi instrument. A monochromatic Al $K\alpha$ source of 1486.6 eV X-ray energy, operating at 15 kV and 160 W, was applied for collecting the XPS spectra. The X-ray spot was approximately 0.5 mm in diameter. A takeoff angle of 90° relative to the sample surface was used for analysis, resulting in an analysis depth of approximately 6 nm. The spectrometer pass energy filter was set at 100 eV for survey scans and 20 eV for elemental regional scans. A 20 s argon sputtering etch was required prior to analysis of *as-polished* samples to remove surface carbon. The energy of the Ar^+ ion beam was 3 keV, and the etching rate was approximately 0.4 nm/s calibrated using a Ta_2O_5/Ta reference sample. The relative surface concentrations of different species were determined by integrating their related peak areas above the linear background.

In the case of SIMS analysis, the intensity data correspond to the local concentration at a specific depth, while in the case of XPS analysis, the data are reflective of the average concentration within the analyzed depth of 6 nm.

RBS. The STAR 2MV tandem accelerator (Australian Nuclear Science and Technology Organisation) was used for RBS analysis. 2 MeV He^+ ions were applied at a normal angle of incidence to the sample surface in the form of a 3-mm-diameter collimated beam. The backscattered ions were detected at an angle of 162° using a silicon surface-barrier detector (4-mm-diameter active area) and a multichannel energy analyzer. A charge of 40 μC was acquired for each sample. The RBS data corresponding to a depth of approximately 84

nm (from the surface) were fit using multilayer models generated by *SIMNRA* (version 6.05) software. Consequently, the RBS results are reflective of the average indium concentration within this 84 nm depth.

5. RESULTS AND DISCUSSION

5.1. PIXE. The results of PIXE analysis are shown in Figure 2, for the as-polished specimen involving 0.3 atom % In. The inset on this drawing is an enlargement of the indium-related peak. It is important to note that the analysis depth of PIXE is on the order of micrometers and the resultant peaks reflect the average concentration within that analysis depth. Consequently, the method is predominantly sensitive to the bulk phase, and the related concentration data are considered as bulk-related.

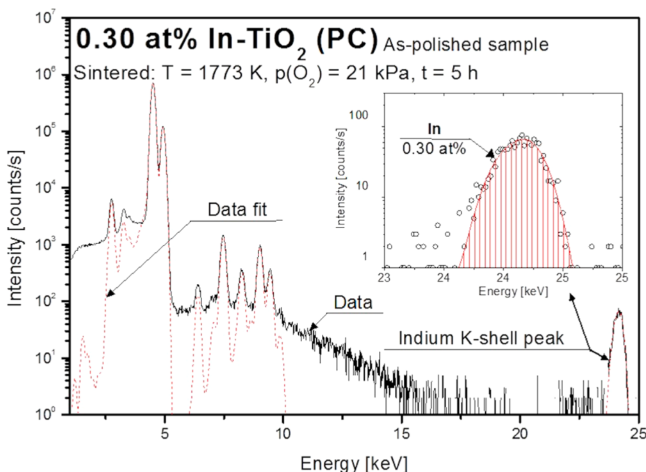

Figure 2. X-ray yield versus energy for the In-doped TiO_2 (0.3 atom %) specimen annealed in the gas phase of $p(O_2)$ = 75 kPa (the inset shows the indium-related peak).

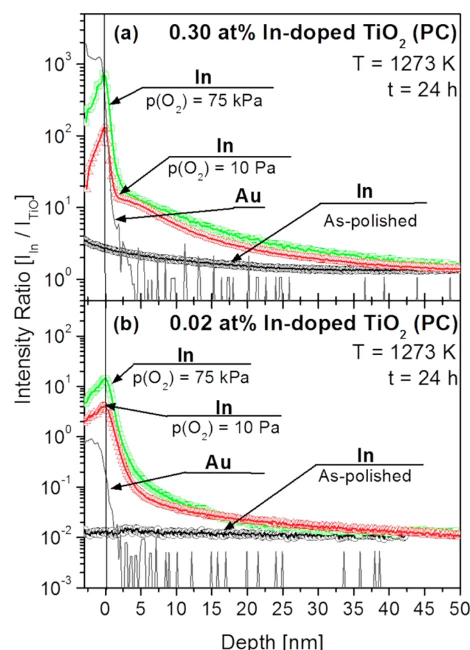

Figure 3. SIMS depth profile for In-doped TiO_2, including the specimen containing 0.3 atom % (a) and 0.02 atom % (b) In, in terms of the intensity ratio of In/TiO secondary ions for as-polished specimens (the reference specimen) and specimens annealed in the gas phases of $p(O_2)$ = 75 kPa and 10 Pa.

5.2. SIMS. The SIMS spectra, represented in the form of the intensity ratio of indium to TiO, are shown in Figure 3. The data can be considered in the following terms: equilibrium vs nonequilibrium depth profile; bulk composition; surface composition.

Equilibrium versus Nonequilibrium Depth Profile. The data on the left side of the vertical line can be considered as nonequilibrium data, which are mainly reflective of the gold layer deposited for the purpose of suppressing the surface charge that is formed during sputtering. The intensity profiles on the right side of this line are reflective of the segregation-induced enrichment of indium (gold profiles are shown as well).

Bulk Composition. The spectrum in Figure 3 for the as-polished specimen, which is relatively flat, essentially corresponds to the bulk phase composition of the sample annealed in air during sintering. Therefore, the related intensity data are considered in the present work as the reference data related to the bulk phase. The observed insignificant increase of the intensity near the surface suggests some minor indium segregation induced by the applied surface polishing procedure and is considered as nonequilibrium segregation.

Surface Composition. As seen in Figure 3, the segregation-induced intensity of indium depends on the oxygen activity. The 0.3 atom % specimen annealed for 24 h at $p(O_2)$ = 75 kPa and 1273 K exhibits the strongest surface enrichment (I_{Ti}/I_{TiO} = ~10^3). The specimen annealed at lower oxygen activity (10 Pa) exhibits a lower surface enrichment (I_{In}/I_{TiO} = ~1.2×10^2). As seen in both cases, a steep initial decrease of the intensity is followed by a change of the slope I_{In}/I_{TiO} versus the depth at 2 nm. The initial part of the intensity versus depth slope, within 1−2 nm, may be considered in terms of a local surface structure, which is different from the rutile structure beneath. In the latter case, the slope is less steep. The observed different intensity versus depth slopes may be considered in terms of different matrices.

As seen, the enrichment concentration profiles converge with the bulk-related profile at 40−50 nm. This value is reflective of the thickness of the surface layer enriched by segregation.

The effect of oxygen activity on indium segregation observed for the 0.3 atom % In specimen is confirmed for the specimen of 0.02 atom %, although the related maxima of the intensity ratios are lower.

The indium enrichment factor in the outermost surface layer may be determined from the intensity ratios between the levels related to the maxima and the level related to the bulk phase (reference specimens). As seen in Table 3, these enrichment factors for the 0.3 atom % specimen assume 486 and 85.3 at higher and lower oxygen activities, respectively. The related enrichment factors for the 0.02 atom % specimen are even larger. These factors are consistent with the tendency of the surface layer to assume a specific composition, independent of the bulk content.[10] However, the enrichment values obtained for the outermost surface layer are markedly larger than those related to XPS. The difference between the two sets of data may be considered in terms of a low-dimensional surface structure, forming one matrix within the outermost surface layer and the rutile structure beneath. This structural difference observed by SIMS is not visible in XPS analysis.

Taking into account the results of the previous work,[14] the low-dimensional surface structure is stable in oxidizing

Table 3. Collection of PIXE, SIMS, XPS, and RBS Data on the Indium Concentration in TiO_2 (Rutile) and the Related Enrichment Factors

		concentration of indium (atom %), enrichment factor $f = [In]_{surface}/[In]_{PIXE}$			
bulk content (atom %)	$p(O_2)$ (Pa)	PIXE	XPS	RBS	SIMS (I_{In}/I_{TiO})
0.30	as-polished	0.30 ± 0.02	0.40 ± 0.08, f_{XPS} = 1.3	0.38 ± 0.08, f_{RBS} = 1.3	1.5
	75 × 10^3	0.29 ± 0.02	2.95 ± 0.6, f_{XPS} = 10.2	2.2 ± 0.4, f_{RBS} = 7.6	729.1, f_{SIMS} = 486
	10	0.29 ± 0.02	2.61 ± 0.5, f_{XPS} = 9.0	1.8 ± 0.4, f_{RBS} = 6.2	128.0, f_{SIMS} = 85.3
0.02	as-polished	0.02 ± 0.004			0.01
	75 × 10^3				14.2, f_{SIMS} = 1420
	10				3.9, f_{SIMS} = 390

conditions. However, imposition of a strongly reducing gas-phase environment results in its decomposition.

5.3. XPS. The XPS spectra for the In-doped TiO_2 specimens, including the *as-polished* specimen and specimens annealed in oxygen and argon, are shown in Figure 4. The related concentration data are shown in Table 3. These data indicate that the surface of the as-polished specimen is slightly enriched in indium to the level of 0.4 atom %. This effect, which is known as nonequilibrium segregation, is related to the applied polishing procedure.

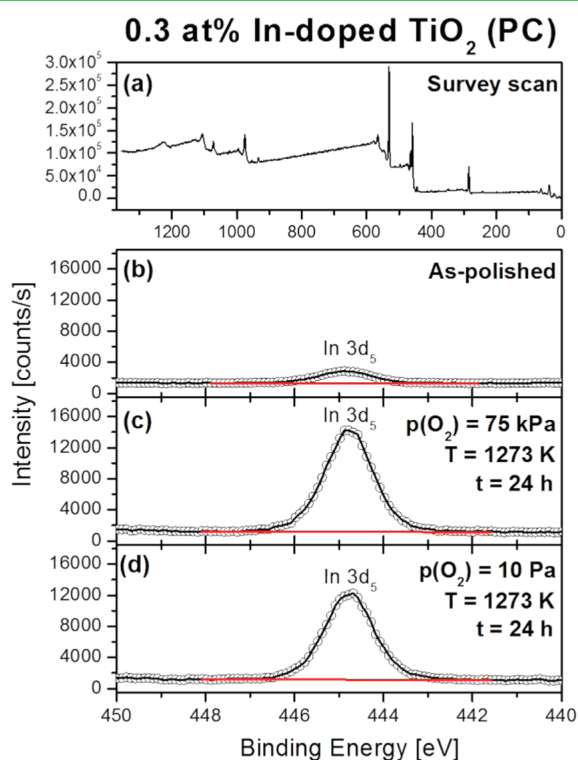

Figure 4. XPS intensity versus binding energy spectra for In-doped TiO_2 (0.3 atom % In), including the survey scan for (a) as-polished (reference specimen) and elemental region scans for (b) as-polished (reference specimen), (c) annealed in the gas phase of $p(O_2)$ = 75 kPa, and (d) annealed at $p(O_2)$ = 10 Pa.

Annealing of the 0.3 atom % specimens at $p(O_2)$ = 75 kPa and 10 Pa (T = 1273 K) results in surface enrichment to the level of 2.95 and 2.61 atom % In, respectively. The respective enrichment factors (10.2 and 9.0) are substantially smaller than those resulting from SIMS (484 and 128, respectively). The difference between these two sets of data is reflective of a very substantial concentration gradient within the surface layer, which is consistent with the postulated low-dimensional surface structure within the outermost surface layer and rutile structure beneath.

5.4. RBS. The RBS spectra are shown in Figure 5 for the *as-polished* reference specimen as well as specimens annealed in the oxidizing gas phase of controlled oxygen activity. The backscattered energy regions of the spectra, which are related to indium, have been enlarged for better clarity.

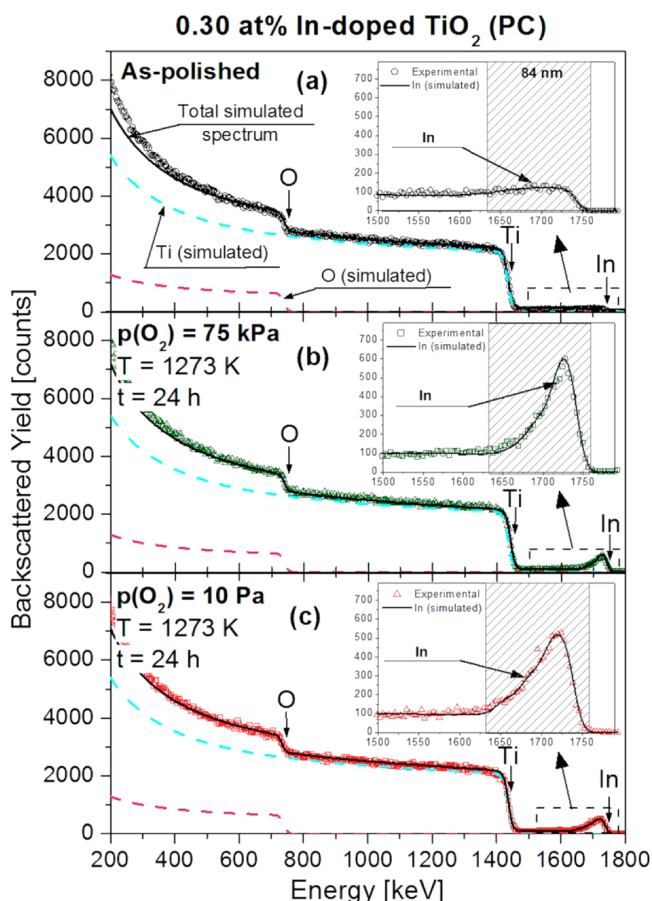

Figure 5. RBS yield versus energy spectra for the following In-doped TiO_2 (0.3 atom %) specimens: (a) as-polished (the reference specimen); (b) annealed in the gas phase of $p(O_2)$ = 75 kPa; (c) annealed in the gas phase of $p(O_2)$ = 10 Pa.

The *as-polished* specimen exhibits 0.38 atom % In. This value, which is slightly lower that that related to XPS analysis (0.4 atom % In), is consistent with the larger RBS analysis depth of 84 nm.

Annealing the specimen at $p(O_2)$ = 75 Pa and 10 Pa (T = 1273 K) results in surface concentrations of 2.2 and 1.8 atom %, respectively. These factors are substantially smaller than

dx.doi.org/10.1021/am301729z | ACS Appl. Mater. Interfaces 2012, 4, 6626−6634

those related to XPS. Again, the difference is consistent with the depth resolution of XPS (6 nm) and RBS (84 nm).

In summary, the determined enrichment factors are reflective of the surface sensitivity of the applied analytical techniques and related depth resolution.

5.5. Theoretical Model. It has been documented in the present work that annealing of In-doped TiO_2 in an oxidizing environment results in indium segregation to the surface. All applied surface-sensitive tools show clearly that the segregation-induced enrichment is enhanced by an increase of the oxygen activity. The most obvious questions that should be addressed at this point are as follows: Why does indium segregate to the surface of TiO_2? Why is indium segregation favored by an increase of the oxygen activity?

Segregation Driving Force. In the first approximation, segregation in oxide solid solutions may be described by the following commonly assumed model, which is based on a regular solution model:[12]

$$\frac{X_2^s}{X_1^s} = \frac{X_2^b}{X_1^b}\exp\left(\frac{-\Delta H_{seg}}{kT}\right) \quad (9)$$

where X is the equilibrium concentration (in mole fraction) of the ith component at the surface (s) and in the bulk phase (b), ΔH_{seg} denotes the heat of solute segregation, and 1 and 2 correspond to the solvent and solute, respectively. The principal contributions to the heat of segregation involve the surface energy contribution and the elastic strain energy contribution. This approach seems plausible because there is a substantial mismatch between the ionic radii of In^{3+} and Ti^{4+} ions (0.081 and 0.068 nm, respectively). While the mismatch explains the tendency for the removal of indium from the bulk due to strain energy, it does not explain why indium segregation is enhanced by an increase of the oxygen activity.

Effects of Oxygen Activity on Indium Segregation. If indium is incorporated into the cation sublattice of TiO_2, the indium ions are charged negatively (compared to the lattice), as expected by equilibrium (4). The segregation of negatively charged indium may be enhanced by increased oxygen activity, if associated with an increase of a positive charge. This is not the case because an increase of the oxygen activity results in an increase of a negative charge associated with the following two effects: (1) formation of negatively charge titanium vacancies, which are located in the outermost surface layer[1] and (2) formation of negatively charged chemisorbed oxygen species, which are located in the adsorbed layer.

The effect of oxygen chemisorption on segregation at elevated temperature may be ignored because the reactivity between oxygen and the TiO_2 lattice in these conditions results in the formation of titanium vacancies. Therefore, only effect (1) can be taken into consideration. This effect is represented schematically by the surface model in Figure 6, showing the concentration of indium versus distance from the surface. This model involves (i) a negatively charged low-dimensional surface structure, which consists of predominantly indium and oxygen, (ii) a negatively charge subsurface layer of TiO_2 enriched in indium, and (iii) a bulk phase of In-doped TiO_2.

Formation of Titanium Vacancies. It has been documented that titanium vacancies are formed at the TiO_2/O_2 interface following the reaction described by equilibrium (4) in Table 2. However, these vacancies are quenched within the outermost surface layer for the kinetics reason. Taking into account the related diffusion data, the diffusion distance of titanium

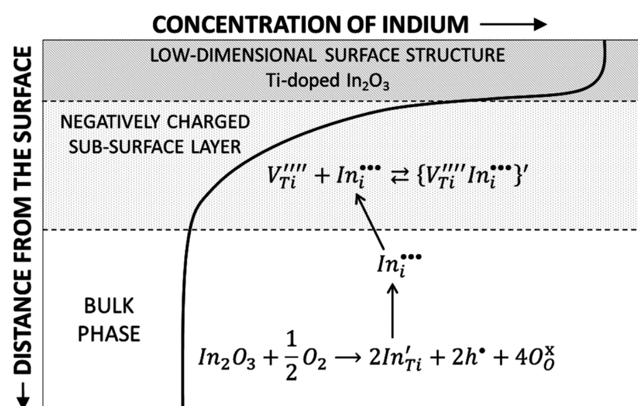

Figure 6. Model representing the surface versus bulk concentration of In-doped TiO_2, in terms of the low-dimensional surface structure, subsurface layer enriched in indium, and bulk phase.

vacancies during the annealing time used in the present work (24 h at 1273 K) is limited to a thin surface layer, while their concentration in the bulk is substantially lower. However, the presence of titanium vacancies at the surface may result in indium segregation only when the effective charge of indium ions is positive. The effect of oxidation on surface versus bulk equilibration of the TiO_2 lattice with respect to titanium vacancies is represented in Figure 7.[29]

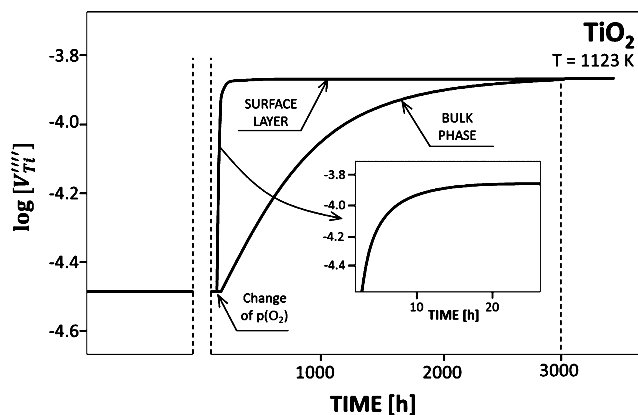

Figure 7. Effect of TiO_2 oxidation on the concentration of titanium vacancies at the surface and in the bulk phase as a function of time at 1123 K.[29].

Surface Mechanism of Indium Incorporation. The reported experimental data indicate that indium is incorporated substitutionally into the bulk phase of the TiO_2 lattice, resulting in the formation of negatively charged species. However, the work of Nakamura et al.[15] has shown that a small portion of indium is incorporated into interstitial sites. In the latter case, the incorporation mechanisms may be represented by the following equilibria:

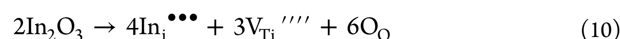

$$2In_2O_3 \rightarrow 4In_i^{\bullet\bullet\bullet} + 3V_{Ti}'''' + 6O_O \quad (10)$$

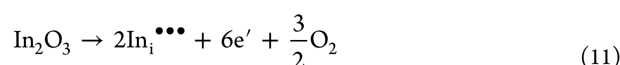

$$In_2O_3 \rightarrow 2In_i^{\bullet\bullet\bullet} + 6e' + \frac{3}{2}O_2 \quad (11)$$

The respective charge-neutrality conditions require that

$$3[In_i^{\bullet\bullet\bullet}] = 4[V_{Ti}''''] \quad (12)$$

$$3[In_i^{\bullet\bullet\bullet}] = n \quad (13)$$

As seen, the mechanism represented by expression (10), which is plausible in the experimental conditions applied in the present work and the associated ionic charge compensation, does not lead to a change in the concentration of electronic charge carriers. On the other hand, indium incorporation according to the mechanism represented by equilibrium (11), which is plausible in reducing conditions, results in the formation of electrons.

According to Nakamura et al.,[15] only a small fraction of indium (11−24%) incorporates into the bulk phase according to the mechanism (10). We postulate in the present work that this mechanism is predominant within the surface layer because of the excess of surface energy and related deformations of the surface layer.[10,11] We believe that this is plausible, taking into account the effect of the excess of surface free energy on the crystal field and the related structural deformations.

It has been shown that defect disorder of the surface layer of metal oxides may be entirely different from that in the bulk phase.[10,11] For example, it has been documented that lithium ions are incorporated into cation sites in the bulk phase of NiO, forming acceptors. On the other hand, lithium is incorporated into interstitial sites, forming donors within the surface layer.[11] In analogy, it has been shown that cobalt ions may be present in interstitial sites within the surface layer of CoO, forming donors, while in the bulk such defects are not stable at all.[11]

The *solubility limit* has been commonly considered as a material-related property. This is the case as far as the bulk phase is concerned. Analysis of the effect of segregation on diffusion indicates that the term *solubility limit* for foreign ions in metal oxides must be considered as the property that is a function of the distance from the surface.[11] The studies of the surface versus bulk properties for Cr-doped CoO have shown that the solubility limit of chromium in the bulk phase at 1000 K is 1 atom % while its solubility within the surface layer is 14 atom % Cr.[26]

In summary, because of the excess of surface energy and related structural deformations, the surface layer may accommodate extraordinary defect disorder and related properties. The experimental data obtained in the present work indicate that the interstitial mechanism (10) should be considered to explain the effect of indium on the properties of the surface layer of TiO_2. At the same time, the substitutional mechanisms, described by the relations (1) and (4), are valid for the bulk phase, and the process of segregation can be considered as a transition of indium from the titanium sites in the bulk to interstitial sites at the surface. This can be described by the following reaction:

$$(\mathrm{In_{Ti}}')_b \rightarrow (\mathrm{In_i}^{\bullet\bullet\bullet})_s + (\mathrm{V_{Ti}}'''')_s \quad (14)$$

The incorporation mechanisms represented by reactions (10)−(14) assume that that the defects in the TiO_2 lattice are isolated and form an ideal solid solution. However, according to Stoneham,[30] an increase of the defect concentration above the level of 0.1 atom % results in substantial defect interactions, leading to the formation of larger defect aggregates. In the case of the present work, the predominant defects at the surface are negatively charged titanium vacancies, which are formed in oxidizing conditions, and positively charged indium ions. These defects are expected to react, leading to the formation of defect complexes:

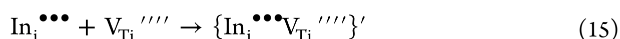

$$\mathrm{In_i}^{\bullet\bullet\bullet} + \mathrm{V_{Ti}}'''' \rightarrow \{\mathrm{In_i}^{\bullet\bullet\bullet}\mathrm{V_{Ti}}''''\}' \quad (15)$$

These complexes have a tendency to form a low-dimensional surface structure, which is charged negatively. The surface composition data according to SIMS analysis, as well as other techniques, indicate that the low-dimensional surface structure, which is formed at the outermost surface layer, is an oxide structure that in the first approximation may be considered as Ti-doped In_2O_3.

Surface versus Bulk Properties. The present work indicates that the mechanism of indium incorporation in the bulk is different from that at the surface. The predominant bulk mechanism results in the formation of acceptor-type centers, which lead to a decrease of the Fermi level in the bulk phase. On the other hand, indium segregation to the surface layer leads to the formation of donor-type ions.

The bulk solubility limit of indium in TiO_2 is in the range 0.4−1 atom % at 1273 K. The determined enrichment data indicate, however, that the indium solubility within the surface layer is markedly larger than that in the bulk phase. The enrichment factor related to the SIMS intensity of indium suggests a low-dimensional surface structure (1−2 nm thick) that resembles a Ti-doped In_2O_3-type structure. This layer is negatively charged.

The near-to-surface layer, just beneath the low-dimensional surface structure, is a solid solution of indium in the rutile structure. Its solubility limit seems to be enhanced at the surface above the level of approximately 1 atom % In. The predominant intrinsic defects in this layer are titanium vacancies and indium incorporated into interstitial sites. The resulting interactions between titanium vacancies and indium ions results in the formation of defect complexes, which are negatively charged. The thickness of the surface layer enriched with indium is approximately 40 nm.

6. CONCLUSIONS

It has been shown that the surface composition of In-doped TiO_2 is entirely different from that of the bulk phase as a result of segregation. The phenomenon of segregation leads to the formation of a strong concentration gradient of indium, which is profoundly influenced by the oxygen activity: the larger the oxygen activity, the larger the segregation-induced enrichment of indium.

Indium incorporates into titanium sites of the TiO_2 lattice, leading to the formation of acceptors in the bulk phase. The related solubility limit of indium in the bulk is in the range 0.4−1 atom %. Indium has a strong tendency to segregate to the surface when annealed in an oxidizing gas-phase environment. The process of segregation involves the removal of indium ions from their titanium lattice sites, transport by an interstitial mechanism toward the surface, and incorporation into interstitial sites.

The solubility of indium in the surface layer is enhanced to the level of approximately 3 atom %. The segregation-induced enrichment of the outermost surface layer results in the formation of a low-dimensional surface structure, which is approximately 2 nm thick, and a sublayer involving defect complexes and larger defect aggregates. Both the low-dimensional surface structure and the sublayer are negatively charged compared to the bulk phase. This negative surface charge is the predominant driving force of indium segregation.

The data reported in the present work show that doping of the TiO_2 lattice with indium results in different effects for the bulk phase and surface layer. While the photoreactivity of TiO_2-based semiconductors and related charge transfer are

dx.doi.org/10.1021/am301729z | ACS Appl. Mater. Interfaces 2012, 4, 6626−6634

determined by the surface properties, knowledge of the difference between the bulk and surface is essential in engineering of the appropriate electric field needed for charge separation.

AUTHOR INFORMATION

Corresponding Author
*Tel: 61-2-4284-7829. Fax: 61-4620-3711. E-mail: J.Nowotny@uws.edu.au.

Notes
The authors declare no competing financial interest.

ACKNOWLEDGMENTS

Thanks are due to Dr. Mihail Ionescu and Ed Stelcer for their guidance with RBS and PIXE analyses. The assistance of Dr. David Nelson with SIMS analysis and Dr. Bill Gong with XPS analysis is sincerely appreciated.

REFERENCES

(1) Bak, T.; Nowotny, J.; Sucher, N. J.; Wachsman, E. *J. Phys. Chem. C* **2011**, *115* (32), 15711−15738.
(2) Fujishima, A.; Hashimoto, K.; Watanabe, T. *TiO_2 Photocatalysis, Fundamentals and Applications*; BKC Inc.: Tokyo, 1999.
(3) Fujishima, A.; Honda, K. *Nature* **1972**, *238*, 37−38.
(4) Carp, O.; Huisman, C. L.; Reller, A. *Prog. Solid State Chem.* **2004**, *32*, 33−177.
(5) Carpentier, J. L.; Lebrun, A.; Perdu, F. *J. Phys. Chem. Solids* **1989**, *50* (2), 145−151.
(6) Karakitsou, K. E.; Verykios, X. E. *J. Phys. Chem.* **1993**, *97* (6), 1184−1189.
(7) Linsebigler, A. L.; Lu, G.; Yates, J. T. J. *Chem. Rev.* **1995**, *95*, 735−758.
(8) Wilke, K.; Breuer, H. D. *J. Photochem. Photobiol., A* **1999**, *121* (1), 49−53.
(9) Burggraaf, A. J.; Winnubst, A. J. A. Segregation in Oxide Surfaces, Solid Electrolytes and Mixed Conductors. *Surface and Near-Surface Chemistry of Oxide Materials*; Elsevier: Amsterdam, The Netherlands, 1988; pp 448−477.
(10) Cabane, J.; Cabane, F. Equilibrium segregation in interfaces. In *Interface Segregation and Related Processes in Materials*; Nowotny, J., Ed.; Trans Tech Publications Ltd.: Zurich, Switzerland, 1991; pp 1−150.
(11) Nowotny, J. Interface defect chemistry and its impact on properties of oxide ceramic materials. In *Science of Ceramic Interfaces*; Nowotny, J., Ed.; Elsevier Science Publishers BV: Amsterdam, The Netherlands, 1991; pp 79−204.
(12) Wynblatt, P.; McCune, R. C. Surface Segregation in Metal Oxides. *Surface and Near-Surface Chemistry of Oxide Materials*; Elsevier Science Publishers BV: Amsterdam, The Netherlands, 1988; pp 247−279.
(13) Nakajima, T.; Sheppard, L. R.; Prince, K. E.; Nowotny, J.; Ogawa, T. *Adv. Appl. Ceram.* **2007**, *106*, 82−88.
(14) Atanacio, A. J.; Nowotny, J.; Prince, K. E. *J. Phys. Chem. C* **2012**, *116* (36), 19246−19251.
(15) Nakamura, S.; Yagi, E.; Osaka, T.; Iwaki, M. *Nucl. Instrum. Methods Phys. Res., Sect. B* **1988**, *33* (1−4), 729−733.
(16) Babu, K. S. C.; Singh, D.; Srivastava, O. N. *Semicond. Sci. Technol.* **1990**, *5* (4), 364−368.
(17) Sasikala, R.; Shirole, A. R.; Sudarsan, V.; Jagannath; Sudakar, C.; Naik, R.; Rao, R.; Bharadwaj, S. R. *Appl. Catal., A* **2010**, *377* (1−2), 47−54.
(18) Wang, E. J.; Yang, W. S.; Cao, Y. A. *J. Phys. Chem. C* **2009**, *113* (49), 20912−20917.
(19) Rodriguez-Gonzalez, V.; Moreno-Rodriguez, A.; May, M.; Tzompantzi, F.; Gomez, R. *J. Photochem. Photobiol., A* **2008**, *193* (2−3), 266−270.
(20) Rangel-Porras, G.; Ramos-Ramirez, E.; Torres-Guerra, L. M. *J. Porous Mater.* **2010**, *17* (1), 69−78.
(21) Iwaszuk, A.; Nolan, M. *J. Phys.: Condens. Matter* **2011**, *23*, 1−11.
(22) Bak, T.; Nowotny, J.; Atanacio, A. J. In progress.
(23) *Solid State Physics*; Kroger, F. A.; Vink, H. J., Eds.; Academic Press: New York, 1956; Vol. *3*, p 307.
(24) Brouwer, G. *Philips Res. Rep.* **1954**, *9*, 366−376.
(25) Atanacio, A. J. Effect of Indium and Niobium Segregation on the Surface vs. Bulk Chemistry of Titanium Dioxide (Rutile). Ph.D. Thesis, University of Western Sydney, Sydney, Australia, 2012; in progress.
(26) Haber, J.; Nowotny, J.; Sikora, I.; Stoch, J. *Appl. Surf. Sci.* **1984**, *17* (3), 324−330.
(27) Doeuff, S.; Henry, M.; Sanchez, C.; Livage, J. *J. Non-Cryst. Solids* **1987**, *89* (1−2), 206−216.
(28) Hirschwald, W.; Loechel, B.; Nowotny, J.; Oblakowski, J.; Sikora, I.; Stolze, F. *Bull. Acad. Pol. Sci., Ser. Sci. Chim.* **1981**, *29* (7−8), 369−375.
(29) Nowotny, M. K.; Bak, T.; Nowotny, J. *J. Phys. Chem. B* **2006**, *110* (33), 16302−16308.
(30) Stoneham, M. *Phys. Today* **1980**, *33*, 34−37.